



Silk Fibroin Nanofibrous Mats for Visible Sensing of Oxidative Stress in Cutaneous Wounds

Journal:	<i>Biomaterials Science</i>
Manuscript ID	BM-ART-08-2020-001325.R1
Article Type:	Paper
Date Submitted by the Author:	02-Sep-2020
Complete List of Authors:	<p>Singh, Sushant; University of Central Florida, AMPAC Cortes, Gabriela; Georgia Institute of Technology Kumar, Udit ; University of Central Florida, Materials Science and Engineering Selvan, Tamil; University of Central Florida, Advanced Materials Processing and Analysis Center (AMPAC), NanoScience Technology Center (NSTC), Materials Science Engineering Niemiec, Stephen; University of Colorado Louiselle, Amanda; University of Colorado Bannerman, Mark; University of Colorado Zgheib, Carlos; University of Colorado Liechty, Kenneth; Children's Hospital Colorado, Seal, Sudipta; University of Central Florida, NanoScience Technology Center; University of Central Florida, Materials Science and Engineering</p>

1 Silk Fibroin Nanofibrous Mats for Visible Sensing of 2 Oxidative Stress in Cutaneous Wounds

3 *Sushant Singh¹, Gabriela Cortes², Udit Kumar¹, Tamil S. Sakthivel¹, Stephen M.*
4 *Niemiec⁴, Amanda E. Louiselle⁴, Mark Azeltine-Bannerman⁴, Carlos Zgheib⁴, Kenneth W.*
5 *Liechty⁴, Sudipta Seal^{1,3*}*

6 ¹Advanced Material Processing and Analysis Center, Department of Material Science and
7 Engineering University of Central Florida, Orlando, FL, 32816

8 ²Dept. of Biomedical Engineering, Georgia Institute of Technology, Atlanta, GA 30332

9 ³College of Medicine, University of Central Florida, Orlando, FL, 32816

10 ⁴Laboratory for Fetal and Regenerative Biology, Department of Surgery, University of
11 Colorado Denver School of Medicine and Children's Hospital Colorado, Aurora, CO,
12 80045

13 *Corresponding Author*

- 1 *Prof. Sudipta Seal* (Sudipta.Seal@ucf.edu)
- 2 Trustee Chair
- 3 University Distinguished Professor and Pegasus Professor
- 4 Chair, Materials Science and Engineering, CECS
- 5

1 ABSTRACT

2 Wound healing is of major clinical concern and is constantly being explored for
3 early restoration and enhanced recovery. While the etiology of the wound healing is
4 multifactorial, high inflammation and increased oxidative stress which results in chronic
5 inflammation, endothelial dysfunction and collagen degradation, delay the overall healing
6 process. Thus, visual sensing of the oxidative stress would be highly informative in the
7 successful implementation of wound healing therapies based on specific requirements.
8 In this study, electrospinning was used to fabricate silk fibroin nanofibrous mats infused
9 with amplex red capable of detecting hydrogen peroxide, a reactive oxygen molecule.
10 These mats produced a visible change in color with the limit of detection at 1 μM H_2O_2
11 concentration. *In vivo* studies carried out in diabetic mice with impaired wounds also
12 displayed a visible change in color of the mats infused with amplex red within 24 hours.
13 These electrospun silk fibroin nanofibrous amplex infused mats has the potential to
14 enable a futuristic platform where decisions can be made for enhanced wound healing
15 therapy.

1 **KEYWORDS:** Wound healing, Oxidative stress, Electrospinning, Silk, Amplex red

2

1 1. INTRODUCTION

2 Cutaneous wounds in general and diabetic wounds in particular have always been of
3 major concern in clinical practice worldwide. Nanomedicine technology has been
4 constantly explored to determine efficient methods for restoring damaged tissues integrity
5 and promote healing, ³. Normal wound repair follows an orderly organized and well-
6 defined sequence of events that requires the interaction of many cell types and growth
7 factors, and is divided into 3 main phases, mainly inflammatory, proliferative, and
8 remodeling phases⁴. At the site of a wound, during an early inflammatory response, the
9 inflammatory cells such as neutrophils and macrophages are highly recruited to the site
10 of injury and destroy potential pathogen by phagocytosis and the productions and release
11 of antimicrobial peptides, proteases and reactive oxygen species (ROS)^{5, 6}. ROS are the
12 by-products of oxygen metabolism and are produced by a variety of cells at the site of
13 inflammation such as platelets, white blood cells, and the mitochondria. The ROS are
14 capable of oxidative killing of bacteria that infiltrate the wound arena. The different ROS
15 molecules produced are superoxide dismutase (O_2^-), hydrogen peroxide (H_2O_2), hydroxyl

1 radical ($\bullet\text{OH}$), peroxynitrite (ONOO^-), that are neutralized by the cellular antioxidant
2 molecules like superoxide dismutase (SOD), catalase (CAT) and peroxidases within the
3 cellular system⁷. The ROS molecules also play an important role in cellular signaling and
4 initial wound healing. ROS activity stimulates the cytokinin and chemokine-receptor
5 activation and hypoxia induces cytokine release⁸. Overall, the combination of these
6 effects attracts the major components of the immune system defense mechanism against
7 invading pathogens. However, in certain cases where normal wound healing is impaired,
8 such as diabetic wounds, the excess amount of ROS can cause damage to proteins,
9 DNA, lipids, and carbohydrates as well as inducing endothelial dysfunction (i.e cellular
10 senescence and fibrotic scarring) and further tissue damage. This process is overall
11 referred to as oxidative stress condition^{7, 9, 10}. Oxidative stress has been implicated with
12 numerous diseases including Parkinson's and Alzheimer's disease, cardiovascular
13 disease, cancer, and wounds¹¹. The wound environment must be accounted for in order
14 to ensure proper healing of wound. Current solutions generally include developing
15 therapeutic regimens to correct and enhance wound healing, however little or no
16 consideration is given to monitoring the wound micro-environment and systemic

1 limitations such as ROS levels, which affect how fast these wounds will heal¹². The ROS
2 levels are measured *in vitro* using cultured cells or *in vivo* by collecting the wound
3 exudates or fluid¹³. Microplate readers and Flow cytometers are generally employed for
4 estimating the amount of ROS in these fluids, and although they provide accurate
5 measurements of these levels, they are not capable of providing the real-time status of
6 the ROS levels within the wound environment,¹⁴⁻¹⁶. Electron paramagnetic resonance
7 (EPR) Spin Trapping spectroscopy is considered the gold standard for measuring the
8 oxygen-based ROS molecules in a biological system. However, limitations could include
9 the formation of EPR silent products when ROS are measured in cells and tissues,
10 leading the failure to detect low level of ROS generation^{17, 18}. Herein, as a proof of
11 concept, we propose a method that gives a visible change in color that can quickly provide
12 a quick measurement of ROS levels in real-time in the wounds. This method detects the
13 level of oxidative stress in a wound site and facilitates the decisions on drugs to be
14 introduced and further interventions required. Amplex red is a highly sensitive and stable
15 fluorogenic probe used to detect and quantify H₂O₂. The detection of H₂O₂ relies on the
16 oxidation of amplex red into resorufin in the presence of peroxidase (**Figure 1**). Amplex

1 red is colorless and non-fluorescent compound, but reacts in 1:1 ratio with H_2O_2 to
2 produce the highly fluorescent resorufin and can detect as little as 10 picomoles of H_2O_2
3 in about 100 μ L volume¹⁹. Reports have shown that when used in an assay, there is a
4 visible change in color from clear solution to pink/purple which is ideal in laboratory
5 settings to ensure a color change is due to H_2O_2 presence^{20, 21}. This amplex red is
6 commonly used for *in-vitro* work, we chose it to be the dye to prove the feasibility of our
7 proof of concept using electrospun silk fibroin nanofibrous mats. The material used for
8 electrospinning with amplex red was silk obtained from *Bombyx mori* silk cocoons. Silk
9 fibroin has been used in several biomedical applications including sutures in surgeries,
10 linen, and hydrogels for tissue engineering²². Biomedical applications of silk fibroin are
11 enabled due to characteristics of the material that make it suitable for these purposes,
12 including robustness, easy chemical modification of surface properties, good
13 biocompatibility, and slow degradation²³.

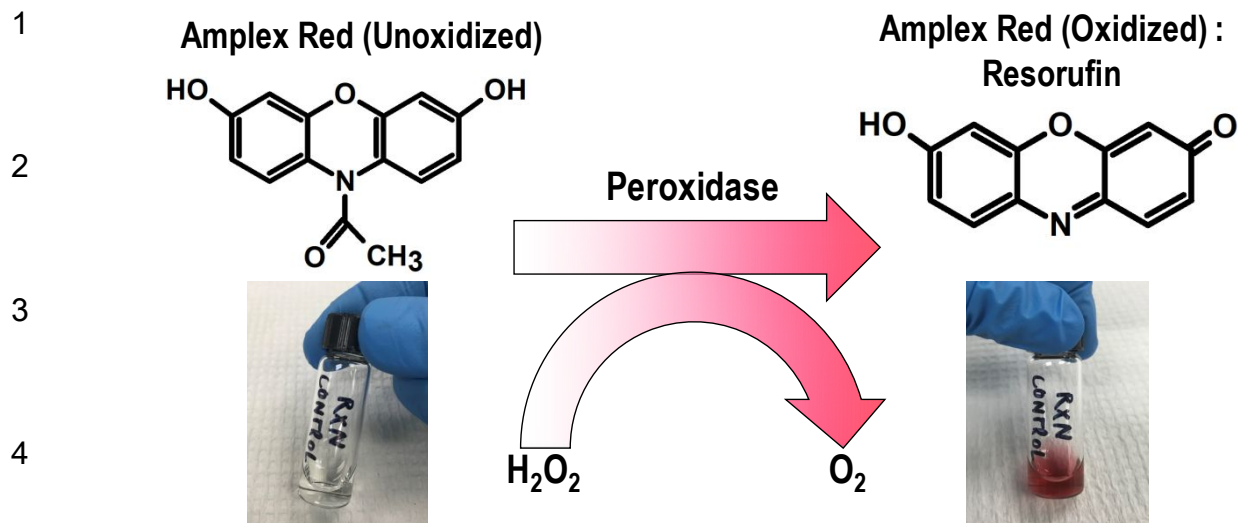


Figure 1: Schematic representation of oxidation of Amplex Red in the presence of Peroxidase and H_2O_2 into a visible color product. Interaction of Amplex Red reagent with H_2O_2 in the presence of Peroxidase leads to its oxidation into a visible pink colored compound Resorufin. Here, this reaction is presented where the vial containing Amplex Red and Peroxidase interaction remains colorless. However, the addition H_2O_2 leads to the instantaneous oxidation of Amplex Red into a highly visible pink colored Resorufin compound.

Silk fibroin nanofibrous mats were fabricated using electrospinning technology leading to the deposition of evenly distributed micro to nano diameter ranged silk nanofibers into mats. This process is highly useful in controlling the surface morphology and other

1 material properties and also offers the flexibility to incorporate substances of interest such
2 as organic dyes like amplex red in our case²⁴. Thus, we propose that integrating amplex
3 red in silk fibroin solution and fabricating electrospun silk fibroin nanofibrous mats will
4 provide a method of visible and rapid detection of ROS level in external wound
5 environment and will provide an insight into the overall wound healing process.

6 **2. MATERIALS AND METHODS**

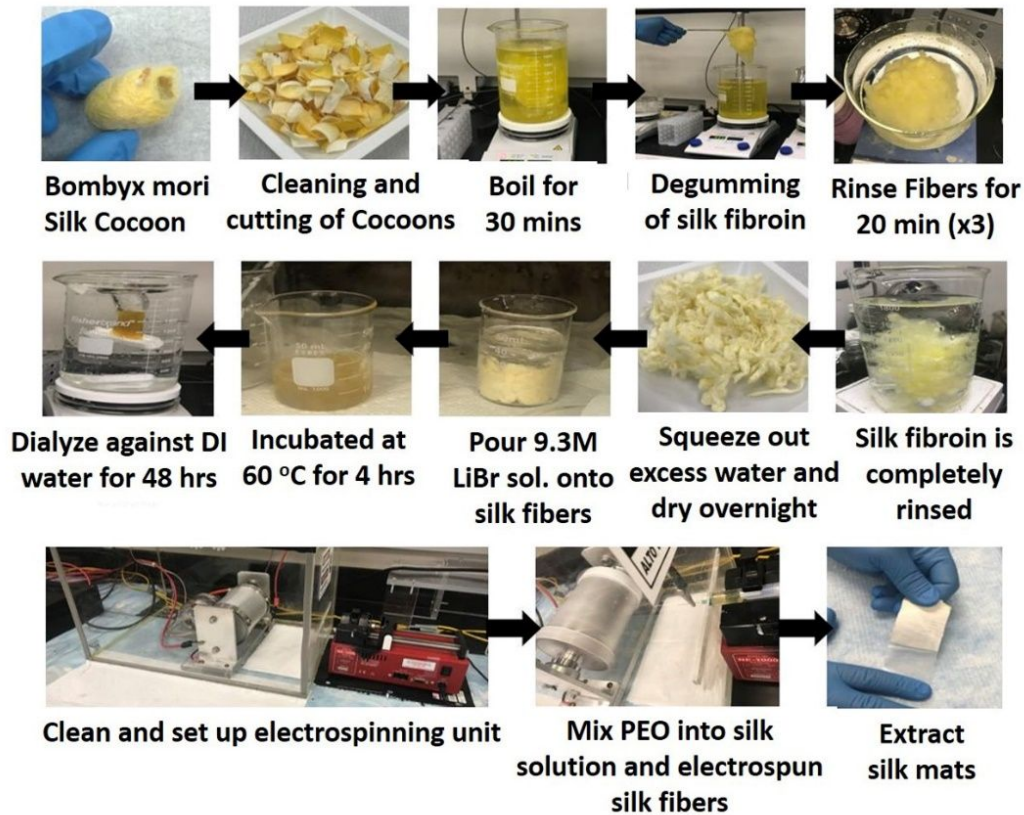
7 **2.1 Preparation of silk fibroin** - Silk fibroin solution was prepared according to the earlier
8 reported protocol²³. In detail, silk cocoons, isolated from *Bombyx mori* silkworms
9 (Technical grade, Aurora Silk, USA) were weighted 5 g, cut into small dime sizes and
10 were degummed using boiling water for 30 minutes containing 0.02 M Na₂CO₃. The
11 degummed silk was washed thrice for 20 minutes each and left further dried out
12 completely. Lithium bromide (LiBr) solution of 9.3 M was prepared, and the dried and
13 degummed silk was incubated in an oven at 60 °C for 4 hours, to prepare the silk fibroin
14 solution. Post incubation, an amber colored and highly viscous silk fibroin solution is
15 obtained. This solution was further dialyzed using ultrapure water for 48 hours. Further,

1 this silk fibroin solution was centrifuged at 9000 rpm to remove the impurities. Finally, a
2 clear and amber colored aqueous silk fibroin solution was obtained with an average silk
3 fibroin concentration of 7% (wt/vol) and stored at 4 °C for further experimental use.

4 **2.2 Fabrication of silk fibroin mats and amplex infused silk fibroin mats using**
5 **electrospinning** - Clear and amber-colored silk fibroin solution collected in previous step
6 was used further to fabricate nanofibrous mats using electrospinning methodology. An
7 appropriate amount of silk fibroin solution was taken into a clean glass vial and 1 mL of
8 5% polyethylene oxide solution (PEO) was mixed into it, under the mild stirring condition
9 for 15 minutes. This solution was drawn into a 5 mL syringe attached to 23G needle and
10 mounted to the syringe pump unit. The electrospinning unit was grounded with positive
11 voltage lead connected to the solution containing syringe needle and the ground lead to
12 the collector surface. The flow rate is adjusted to 1 mL/hr and the current was set to 2 A
13 and electric potential at 20 KV. The distance between the syringe needle and the collector
14 drum was set to 10 cm apart. Speed of the collector drum was set at 2000 rpm.
15 Electrospinning of silk fibroin mats was performed till a visible mat of suitable thickness

1 gets collected onto the collector unit (**Figure 2**). The silk fibroin nanofibrous mats
2 synthesis here will be used as control mats for different experimental purpose. Similar to
3 this, amplex red infused silk fibroin nanofibrous mats were fabricated using electrospinning
4 technique. In this process, the stock of amplex red solution was prepared in DMSO firstly at a
5 concentration of 5 mg/mL. From this stock, 1 mL of amplex red solution was added to the 45 mL
6 of silk fibroin solution (Silk concentration - 54.4 mg/mL) under mild stirring condition in
7 increment of 200 μ L every 5 minutes. This Amplex red-Silk fibroin solution was stored under 4
8 $^{\circ}$ C and used for electrospinning of nanofibrous silk fibroin mats using the above-mentioned
9 protocol. Similarly, control nanofibrous silk fibroin mats were also prepared using silk fibroin
10 solution only.

11



1 **Figure 2:** Schematic representation of the Silk fibroin preparation from raw silk cocoons through
 2 degumming process and solubilization. Electrospinning of silk fibroin solution leads into the
 3 formation of nanofibrous silk fibroin mats.

4 **2.3 Characterization of silk fibroin nanofibrous mats synthesized with and without amplex.**

5 - Surface morphology of the nanofibrous silk fibroin mats and amplex infused nanofibrous silk
 6 fibroin mats were examined using scanning electron microscope (Zeiss ULTRA-55 FEG scanning
 7 electron microscope). For SEM imaging purpose, these mats were sputter-coated with a thin layer
 8 of gold and were placed on imaging stub and recorded. To further characterize these nanofibrous
 9 silk fibroin mats, Fourier Transform Infrared Spectroscopy (FTIR) was also carried out using

1 Perkin Elmer Spectrum-I instrument at room temperature in ATR mode from 4000-650 cm^{-1} . X-
2 ray photoelectron spectroscopy (XPS) analysis was also conducted using an ESCALAB-250Xi
3 spectrometer in an ultra-high vacuum chamber (below 7×10^{-9} mbar) using an Al-K α
4 monochromatic radiation source, operating at a power of 300 W (15 kV, 20 mA). Binding energies
5 were calibrated based on C1s peak at $284.6 \text{ eV} \pm 0.2 \text{ eV}$ and the chemical functional groups were
6 identified and deconvoluted using Thermofisher Avantage software.

7 **2.4 *In-vitro* cellular biocompatibility analysis-** Amplex red compound was tested for *in vitro*
8 cellular toxicity analysis against the human skin keratinocyte (HaCat) cells (purchased from
9 ATCC, USA) using cell culture-based MTT assay method. Herein, 10,000 cells were grown
10 overnight in a 96 well plate using DMEM:F12 cell culture media. Different concentration of
11 amplex red compound was prepared using only basal DMEM/F12 cell culture media and incubated
12 with HaCat cells for a time period of 24 hours and 48 hours respectively. Post incubation time
13 period, MTT analysis was performed using the standard protocol described in an earlier
14 publication²⁵. MTT assay compound was then (Thiazyolyl blue tetrazolium bromide) added for
15 measuring the cellular viability and absorbance was recorded for treated in comparison to control
16 samples (HaCat cell only) and data analysis was performed.

17 **2.5 H_2O_2 detection assay and Limit of detection (LOD) analysis-** Silk fibroin nanofibrous mats
18 infused with or without amplex were tested for a visible change in color as a detection parameter
19 of hydrogen peroxide. For this assay, phosphate buffer saline (PBS), horseradish peroxidase
20 (HRP), and H_2O_2 solution were prepared. HRP stock solution was made by resuspending it to a
21 concentration of 5 mg/mL, as per requirement. 3% H_2O_2 stock solution was diluted to make it a
22 1% H_2O_2 solution and placed in a conical tube wrapped in aluminum foil, avoiding direct light.
23 Further dilutions of these H_2O_2 and HRP were made from these stocks as per requirement using

1 PBS. The visible change in color reaction was optimized using 1 mL PBS and 100 μ L 2.5 mg/mL
2 HRP. The control reaction vial had 10 μ L of amplex red reagent (5 mg/mL) added to it. Once these
3 vials were prepared, 100 μ L of 1% H₂O₂ were added to all vials and the visible change in color
4 was recorded. To determine the LOD, different concentrations of HRP and H₂O₂ were prepared.
5 Control silk fibroin mats and amplex red infused silk fibroin mats of similar sizes (1 cm x 0.5 cm
6 size) were placed in a 12-well plate. In each well, 1 mL of PBS, 50 μ L of specified HRP
7 concentration, and 50 μ L of specified H₂O₂ concentration were added. These nanofibrous mats
8 were imaged for visible change in color development at different time points and further analysis
9 was carried out using ImageJ software. (ImageJ version 1.52a (National Institute of health, USA;
10 <http://imagej.nih.gov/ij>)

11 **2.6 *In-vivo* animal experiments for visible change in color detection of H₂O₂** - All experimental
12 protocols were approved by the Institutional Animal Care and Use Committee at the University of
13 Colorado Denver—Anschutz Medical Campus and followed the guidelines described in the NIH
14 Guide for the Care and Use of Laboratory Animals. Age-matched, female, genetically diabetic
15 C57BKS.Cg-m/Leprdb/J (Db/Db) mice were used in these experiments. To examine the ability of
16 silk fibroin nanofibrous mats infused with amplex red to detect oxidative stress *in vivo*, 12-week-
17 old Db/Db mice were anesthetized with inhaled isoflurane and shaved before wounding. The
18 dorsal skin was sterilized with alcohol and Betadine (Purdue Pharma, Stamford, CT). Each mouse
19 underwent a single, dorsal, full-thickness wound (including panniculus carnosum) with an 8-mm
20 punch biopsy (Miltex Inc., York, PA). One set of the wounds was covered with amplex infused
21 silk fibroin nanofibrous mats and another set was covered with a control silk fibroin nanofibrous
22 mats only. All wounds were then dressed with Tegaderm (3M, St. Paul, MN), and pictures of the

1 wounds were taken directly after the mats were applied, and at 3, 4, 5, and 24 hours post-
2 application.

3

4 **3. RESULTS AND DISCUSSION**

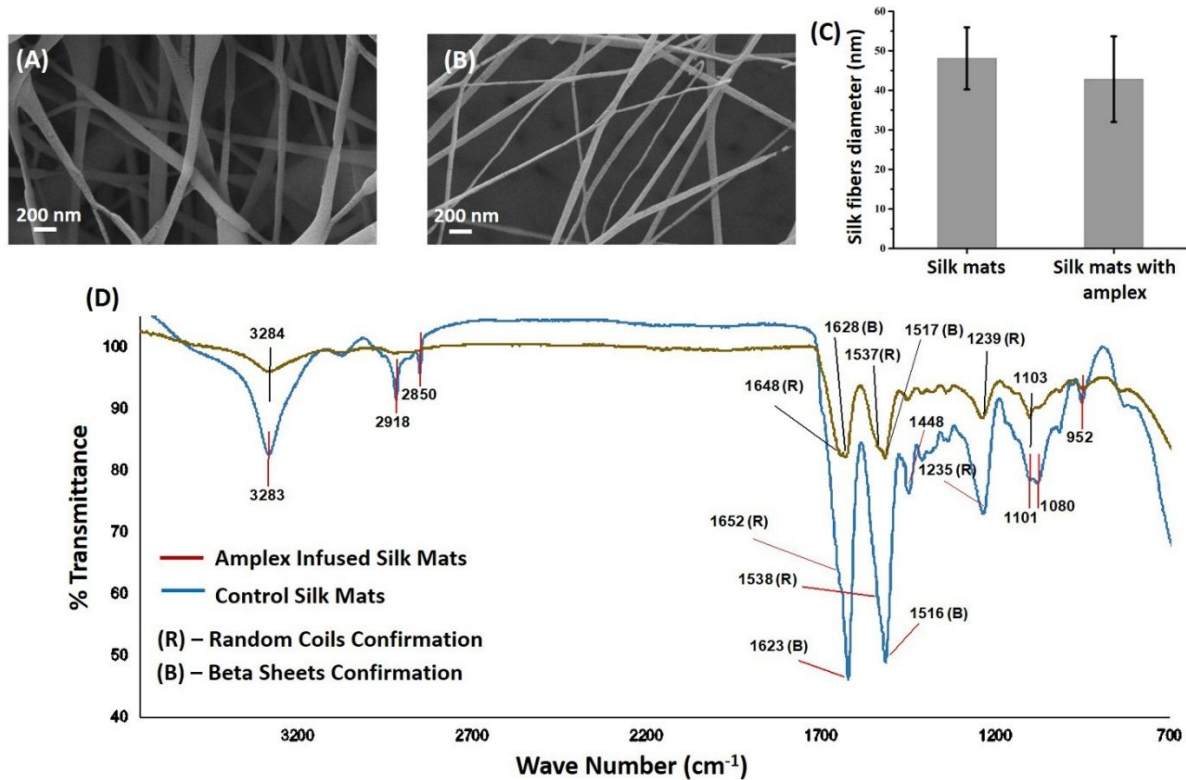
5 The major hypothesis behind this work was to fabricate a flexible electrospun silk fibroin
6 nanofibrous mat which is highly sensitive to oxidative stress environments and can visibly detect
7 the presence of hydrogen peroxide with a change in color, especially when applied on cutaneous
8 wounds. This hydrogen peroxide sensing platform would be used to determine efficient therapies
9 based on the wound healing stage.

10 **3.1 Electrospinning of Silk fibroin nanofibrous mats and SEM, FTIR characterization.** In
11 this direction, a highly clear and semi-viscous silk fibroin solution was prepared from raw silk
12 *Bombyx mori* cocoons employing the previously established protocol for fabricating electrospun
13 silk fibroin mats^{23, 26}. This preparation of silk fibroin is desired because the final silk fibroin
14 solution is in an aqueous state and provides the flexibility of doping with any external materials or
15 compound. As such, in this study amplex red is doped into the silk fibroin solution prior to
16 electrospinning. Using the drying technique, the concentration of silk fibroin solution obtained
17 was 7%. These silk fibroin solutions were processed for electrospinning by mixing with 5mL of
18 5% polyethylene oxide (PEO) before electrospinning. It has been reported that PEO addition
19 to silk fibroin solution induces ample surface tension and sufficient viscosity so that a
20 continuous fibroin jetting can be maintained, a requirement for the efficient

1 electrospinning of nanofibrous mats^{27, 28}. The silk fibroin nanofibrous mats were electrospun
2 from the silk fibroin solution blended with polyethylene oxide (PEO), which is also a
3 biocompatible polymer²⁹⁻³¹. This also minimizes the potential toxicity which may arise from the
4 use of any organic solvent and may later affect the applicability of these mats *in vitro* and *in vivo*.
5 Silk fibroin electrospinning was performed using the electrospun setup (**Figure 2**) and silk fibroin
6 nanofibrous mats (Control) were obtained on the metal collector unit. Similarly, both amplex
7 infused silk fibroin nanofibrous mats were synthesized through electrospinning technique. These
8 electrospun control silk fibroin mats and amplex infused silk fibroin mats were processed further
9 in small sizes for SEM, FTIR and biochemical testing. The electrospinning technique was applied
10 because it creates numerous beneficial features in these mats including high porosity created by
11 the electrospun nanofibers which helps in the absorption of the exudates in the wound and efficient
12 gas exchange which supports the wound cells migration and promote cellular proliferation. Also,
13 the amplex red has been exclusively used for the detection of H₂O₂ in solutions with a detection
14 limit as low as 10 picomolar. Amplex red is an ultrasensitive compound used in combination with
15 HRP for the quantitative determination of hydrogen peroxide as a marker of oxidative stress.
16 Combination of amplex red and HRP has been used to estimate the H₂O₂ generation in native and
17 recombinant microsomal preparations of cytochrome P450³². Similarly, amplex red has been used
18 for estimating oxidative stress through H₂O₂ in polymeric hydrogel spheres^{33, 34} as well in
19 mammalian cell culture system of human respiratory epithelial A549 cells³⁵. The infusion of silk
20 fibroin solutions with different compounds and dyes and electrospun into nanofibrous silk fibroin
21 mats have also been reported. It has been reported that applicable dyes or drug agents can be

1 successfully infused into the silk fibroin nanofibers during the electrospinning process including
2 FITC-albumin and riboflavin^{36, 37}. Infusion of these molecules into electrospun nanofibers
3 indicates that successful incorporation of amplex red into the silk fibroin nanofiber can be
4 achieved, which was further confirmed using the physiochemical characterization of the
5 synthesized mats.

6 Electrospinning is a versatile technique allowing the formation of scaffolds which is ultra-
7 structurally composed of highly porous micro/nanofibers arranged in uniform fashion depending
8 on the electrospinning unit collector setup^{38, 39}. Here, the control electrospun nanofibrous silk
9 fibroin mats and the amplex-red infused nanofibrous silk fibroin mats were subjected to
10 physiochemical and biochemical characterization. SEM was used to image the nanofibrous
11 ultrastructure and identify if the infusion of amplex red had any effect on the nanofibrous diameter
12 during its electrospinning process and ultimately silk fibroin mats formation. Fine silk fibroin
13 nanofiber images were observed at a scale bar of 200 nm with the average nanofiber diameter
14 around 50 nm. Similar nanofibre ultrastructure was also observed in both control and amplex
15 infused silk fibroin nanofibrous mats (**Figure 3A-C**).



1
 2 **Figure 3:** Electrospun silk fibroin nanofibrous mats with and without amplex were characterized
 3 using scanning electron microscope (SEM). SEM analysis indicates the formation of continuous
 4 silk fibroin nanofibers leading to a synthesis of electrospun silk fibroin mats. A) represents the
 5 nanofibrous silk fibroin mats while B) represents nanofibrous silk fibroin mats infused with
 6 Amplex red. Formation of ultra-fine continuous nanofibers can be observed in both of these silk
 7 fibroin mats. C) Shows a bar graph of the nanofiber size measurement (from SEM images) using
 8 ImageJ analysis of the 10 different nanofibers in each sample. The addition of amplex red does
 9 not have any significant effect on the nanofiber's diameter. D) FTIR analysis was also performed

1 on silk fibroin mats and Amplex red infused silk fibroin mats. The presence of amide region peaks
2 in the range of 1600 cm^{-1} , 1500 cm^{-1} and 1200 cm^{-1} indicates the presence of random coils and
3 beta sheets conformations of silk fibroin indicating the aqueous stability of nanofibers. The
4 presence of other specific peaks in the region of 2900 cm^{-1} , 2800 cm^{-1} , 1000 cm^{-1} and 950 cm^{-1}
5 indicates the infusion of Amplex Red compound into the nanofibrous silk fibroin mats. (R)
6 represents the random coils conformations of the silk fibroin while (B) represents the beta-sheets
7 conformation bands of the silk fibroin.

8 The control silk fibroin mats and amplex infused silk fibroin mats, both were having
9 the similar nanofibrous ultrastructure indicating the lack of any effect of amplex red
10 infusion before electrospinning. The nanofiber diameter of silk fibroin depends upon the
11 route of materials synthesis, solvent types and ultimately electrospinning parameters.
12 Reports indicated that nanofiber diameter can vary from 100 nm to maximum 1000 nm
13 using the aqueous-based electrospinning of silk fibroin mats. Here we too developed the
14 aqueous-based silk fibroin solution and nanofiber diameter obtained was less than
15 reported earlier^{40, 41}. It is also important to identify the chemical nature of the silk fibroin
16 mats and for this FTIR analysis was performed on the both the control silk fibroin

1 nanofibrous mats and the amplex red infused silk fibroin nanofibrous mats (**Figure 3D**).

2 The FTIR spectra obtained for both these silk fibroin mats were compared and analyzed.

3 The 1103 cm^{-1} band, likely caused by the C-C stretching of tyrosine aromatic rings,

4 tryptophan or phenolic compounds, also appeared in previous studies on *Bombyx mori*

5 silk characterization, and it appeared in the FTIR spectra of both of the control silk fibroin

6 mats and amplex infused silk fibroin mats⁴² Amide regions peaks (Amide I, II, III) in the

7 zone 1600 cm^{-1} , 1500 cm^{-1} and 1200 cm^{-1} were highly prominent in both types of silk

8 fibroin nanofibrous mats, indicating the presence of random coils and beta-sheet

9 conformation. The electrospun silk fibroin nanofibrous control mats were composed of

10 both the Silk-I (Random coils) and Silk-II (β -sheet conformation) of silk fibroin. The FTIR

11 data of control silk fibroin mats (Figure 3D) indicates the characteristic band peaks for

12 these random coils conformation (1648 cm^{-1} , 1537 cm^{-1} , 1239 cm^{-1}) and β -sheet

13 conformation (1628 cm^{-1} , 1517 cm^{-1})^{43, 44}. Reports have indicated that despite an intense

14 band at 1650 cm^{-1} of Silk-I/random coils conformation, there is subtle amount of Silk-II/

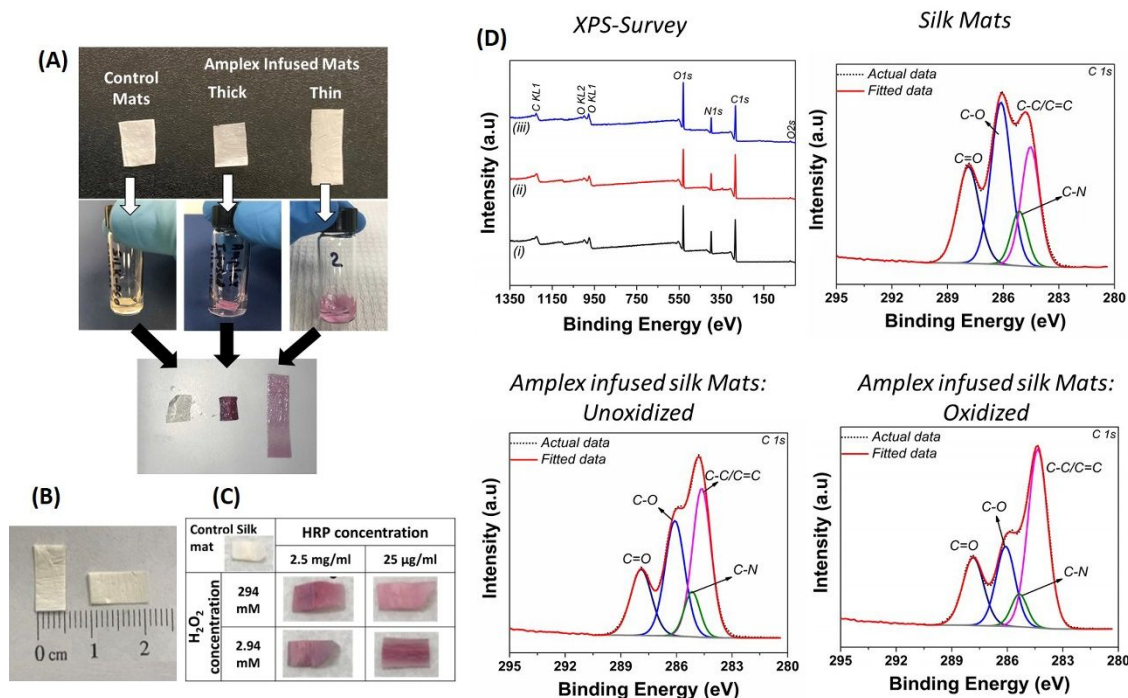
15 beta-sheet conformation present with less intense bands at 1622 cm^{-1} . Thus, it's expected

16 for electrospun silk fibroin mats to show preferentially random coil conformations but in

1 coexistence with a minor proportion of beta-sheet structures^{43, 45}. Also, the FTIR peaks of
2 amplex infused silk fibroin mats were in close coincidence with control silk fibroin mats.
3 Amplex infused silk fibroin mats contained high-intensity peaks in the 1623cm^{-1} , 1516cm^{-1}
4 $^{-1}$ region corresponding to beta sheets structure and this is due to the interaction between
5 DMSO present into amplex red solution and silk fibroin when added for electrospinning⁴⁵.
6 FTIR analysis also indicates that the control silk fibroin samples band were minor at 1628
7 cm^{-1} and 1517cm^{-1} , while the amplex containing silk fibroin sample has a sharper band at
8 1623cm^{-1} and 1516cm^{-1} , indicating the random coil transformation into β -sheet structures
9 by the DMSO used for solubilizing amplex compound for electrospinning the mats.
10 Additional FTIR peaks appeared into the amplex infused silk fibroin mats which might be
11 due to the presence of the amplex compound within the silk fibroin nanofibrous mats
12 **(Figure 3D)**. The FTIR peaks at 1400 cm^{-1} indicate the OH alcohol group bending, 1080
13 cm^{-1} indicate the C-O alcohol stretch while 953 cm^{-1} indicate the C=C stretch, specific
14 functional groups associated with the amplex red compound. The presence of these
15 functional groups into the amplex infused nanofibrous silk fibroin mats indicate the high
16 infusion rate and retention of the complete chemical moiety of the amplex compound even

1 after the electrospinning procedure. Amplex retention is further confirmed through the
2 biochemical testing which induces the visible color change immediately upon
3 encountering the H_2O_2 and peroxidases, indicating the robustness of the chemical
4 compound even through passing the high potential differences during the electrospinning
5 process.

6 **3.2 In vitro testing and XPS analysis of Control and Amplex-infused Silk fibroin**
7 **nanofibrous mats.** The chemical integrity of amplex infused silk fibroin mats was further
8 tested with a visible change in color for sensing H_2O_2 moiety in solution. Both control silk
9 fibroin mats and amplex infused silk fibroin mats were tested using HRP and H_2O_2 for
10 visible change in color from a transparent solution into pink/purple color. The amplex-
11 infused silk fibroin mats were found to gets oxidized and produced a visible pink color
12 immediately upon interaction with HRP and H_2O_2 compounds (**Figure 4A**). It has been
13 reported that amplex red limit of detection for H_2O_2 is to 10 picomoles under specified
14 conditions, which is much lower than the normal physiological H_2O_2 concentration within
15 a cellular system.



1

2 **Figure 4:** Amplex Red compound infused Silk fibroin nanofibrous mats is being tested as a proof

3 of concept for the visual detection of H₂O₂. A) represent control (silk fibroin mats) and Amplex

4 infused silk fibroin mats (Thick~0.0043mm thickness and Thin one ~0.001mm thickness) being

5 tested. The thick and thin nanofibrous silk fibroin mats efficiently develop the pink color through

6 the oxidation of Amplex red into Resorufin. B) represents the dimensions of electrospun silk

7 fibroin mats used for further sensing measurement. These dimensions were 1x0.5 cm (length x

8 height) for sensing measurements. C) Amplex Infused silk fibroin mats treated with 2 different

9 concentrations of H₂O₂ and HRP were kept at 100 folds apart in concentration. A control mat is

10 shown at the top left corner for color development comparison. The mats efficiently develop the

1 visible color on being treated with hydrogen peroxide. D) Surface elemental analysis of control
2 silk fibroin mats, Amplex Infused silk fibroin mats, and Amplex Infused silk fibroin mats that have
3 undergone a color change through the oxidation of Amplex red component. Survey spectra (i) Silk
4 fibroin mats, (ii) Amplex infused silk fibroin mats: unoxidized, and (iii) Amplex infused silk fibroin
5 mats: oxidized and C 1s spectra of respective silk fibroin mats with the deconvolution of the
6 experimental spectra results in peaks corresponding to the binding energy of C-C/C=C, C-N, C-
7 O and C=O. Fitted and actual spectra are shown.

8 Amplex red oxidation into resorufin indicated its successful infusion within the silk
9 fibroin ultrastructure and its robust chemical integrity which remains uncompromised
10 during the electrospinning procedure. Amplex red withheld its functional chemical integrity
11 through higher electric potential difference and from aqueous to solid phase. Further,
12 these silk fibroin mats were cut into 1.0 x 0.5 cm dimensions and were tested with HRP
13 and H₂O₂ at 2 different concentration 100-fold apart for the color development and
14 sensitivity. Concentration of HRP was 2.5 mg/mL and 25 µg/mL while H₂O₂ concentration
15 was 294 mM and 2.94 mM (**Figure 4B, C**). It was found that visual color development took
16 place at both the concentration, indicating a highly robust nature of the amplex infused

1 silk fibroin mats and a wide range of sensitivity for H₂O₂ sensing. This analysis also
2 directed us to proceed to lower H₂O₂ concentration for detection. To examine the detailed
3 surface elemental composition, XPS was carried out on the control silk fibroin mats,
4 Amplex infused silk fibroin mats, before and after the oxidation. The corresponding
5 spectral lines are shown in **Figure 4D**. The full survey spectral envelopes of all silk fibroin
6 mats contains C, O, N as the primary elements⁴⁶ with different concentration of atomic %.
7 The relative concentration of C, O, N in the silk fibroin derivatives, quantified from the
8 equivalent photoelectron peak area are presented in **Table 1**. The incremental atomic %
9 of carbon (4.14%) from control silk fibroin mats to Amplex infused silk mats indicate that
10 the amplex red is successfully incorporated within the silk mat. Furthermore, atomic % of
11 oxygen increased from unoxidized amplex infused silk fibroin mats (20.27%) to oxidized
12 silk fibroin mats (24.98%) is the clear evidence of oxidation
13 reaction occurred within the silk fibroin mats.

14

- 1 **Table 1:** Composition (atomic %) of silk fibroin mats, Amplex infused silk fibroin mats: oxidized
 2 and unoxidized, as well as the peak area % of each carbon components identified from C1s

Sample	Atomic %			C1s - Peak area %			
	C1s	N1s	O1s	C-C/C=C	C-N	C-O	C=O
Silk fibroin mats	62.60	15.8 1	21.5 8	25.9	10.4	38.7	25.0
Amplex infused silk fibroin mats: unoxidized	66.74	12.9 9	20.2 7	39.1	9.9	31.7	19.3
Amplex infused silk fibroin mats: oxidized	62.25	12.7 7	24.9 8	50.5	8.5	21.8	19.2

- 3 spectra of respective silk fibroin mats

4

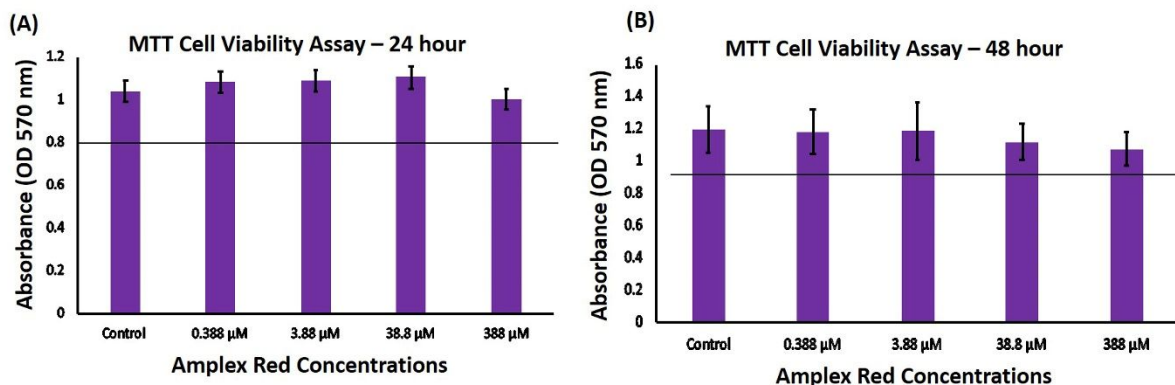
- 5 To understand the associated local environmental modifications around carbon,
 6 the high-resolution C1s envelope was deconvoluted and fitted into four peaks, namely,
 7 C-C/C=C, C-N, C-O, and C=O, centered at 284.5 ± 0.2 eV, 285.14 ± 0.2 eV, 286.12 ± 0.2
 8 eV, and 287.88 ± 0.1 eV, respectively, as shown in **Figure 4D**⁴⁷. C=O attributes the carbon
 9 on the peptide backbone groups associated with β -structures, while C-C/C=C reflects the
 10 aliphatic carbons of the amino acid pendant groups. The integrated peak area ratios (*IPA*

1 $R_i = A_{O_i}/\sum A_{O_i}$ for C-C/C=C, C-N, C-O, C=O are presented in **Table 1**. The changes in the
2 peak area ratio of the different carbon species indicate that reaction occurred within the
3 unoxidized amplex infused silk fibroin mats (before introduction to H₂O₂) and oxidized
4 amplex infused silk fibroin mats (after introduction to H₂O₂ and color development).
5 Similarly, the high-resolution XPS O1s spectra presented in Figure S1 show the
6 associated local environment modification around oxygen and nitrogen. Therefore, it is
7 concluded that amplex is infused into the silk fibroin mats and that a reaction does occur
8 with the oxidation of amplex into resorufin within the silk fibroin mats, indicated with the
9 visible color change.

10 **3.3 Cellular biocompatibility for Amplex compound and Amplex infused nanofibrous silk**

11 **fibroin mats LOD analysis** – Silk fibroin is known to be an excellent biomaterial, it is highly
12 biocompatible and has been in use for generations. It has found its applications in sutures
13 and other biomedical applications. The unique features include the high mechanical
14 strength, biocompatible nature and varied ability of the silk protein to change its structural
15 and morphological features. Silk fibroin is applied across various grafts including skin,

1 bone and vascular tissues^{29, 48, 49}. The silk fibroin mats developed here use amplex red
2 compound for H₂O₂ sensing. It is important to identify the cellular biocompatibility of the
3 amplex red compound and the amplex red infused silk fibroin mats. Cellular
4 biocompatibility was tested using human skin keratinocyte (HaCat) cells employing the
5 standard MTT assay. It was observed that amplex red was completely non-toxic to the
6 cells. The 24 hours and 48 hours MTT data produced the cellular viability beyond 80%
7 which indicate its nontoxic nature at the highest concentration of 388 μ M, indicating its
8 potential application into the cell-based detection system (**Figure 5A, B**). In the previous
9 experiment, HRP and H₂O₂ level were tested across 2 different concentrations of 100 folds
10 apart. The lower level of HRP was 25 μ g/mL while the level of H₂O₂ was 2.94 mM. The
11 visible color development at this concentration of HRP and H₂O₂ were immediate.



1 **Figure 5:** Cellular biocompatibility analysis was performed for Amplex Red compound using the
2 Human Skin keratinocyte (HaCat) cells through measuring the cellular viability by MTT assay.
3 Cellular viability beyond 80% was considered biocompatible. Different concentration of Amplex
4 Red compound was used and concentration up to 388 μM was found to be highly biocompatible
5 when tested for A) 24 hours and B) 48 hours cellular biocompatibility test.

6 The HRP concentration of 25 μg/mL produces a satisfactory and immediate visible
7 color change in the presence of H₂O₂. Further limit of detection for H₂O₂ was analyzed
8 keeping the concentration of HRP constant at 25 μg/mL and thus varying the level of H₂O₂
9 concentration from a higher level of 1 mM to lower level of 1 μM. A total of 8 different
10 concentration were tested for visible change in color with respect to control mats under
11 similar temperature and humidity. The amplex red infused nanofibrous silk fibroin mats
12 developed the visible color change immediately upon H₂O₂ interaction. Although the

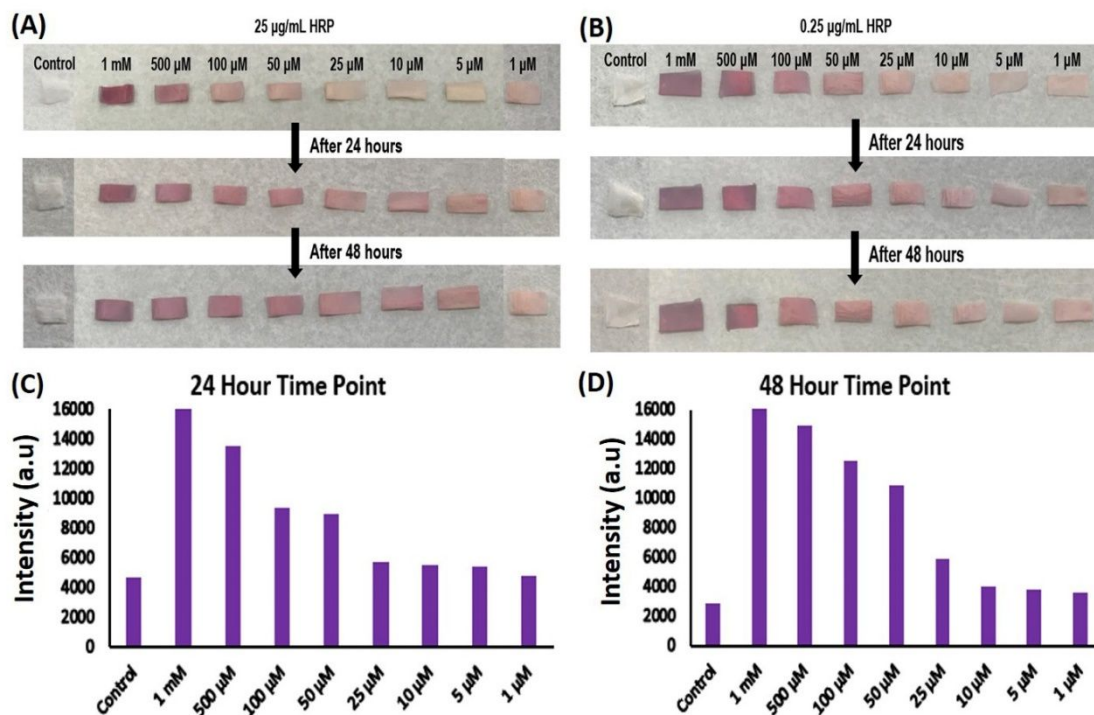
1 visible color change was observed immediately, the analysis was done at 2 different time
2 point of 24 hours and 48 hours. This is done to observe the degree of color change over
3 time duration within the presence of HRP and H₂O₂. Post-incubation we observed that
4 the initial developed visible color intensity did not change after 48 hours. Also, the amplex
5 infused silk fibroin mats at lowest concentration of 1 μM H₂O₂ develops color, indicating
6 the limit of detection to be much lower (**Figure 6A**). The HRP concentration was lowered
7 to 100-fold up to 0.25 μg/mL for further sensitivity analysis. Herein, the visible observation
8 indicated that the color development plateaued at 25 μM of H₂O₂ and at 0.25 μg/mL of
9 HRP concentration (**Figure 6B**). ImageJ software-based analysis measured the color
10 intensity of the silk fibroin mats, indicating the color development even at the lowest
11 concentration (**Figure 6C, D**).

12

13

14

1



2

3 **Figure 6:** Control and Amplex infused silk fibroin mats treated with fixed concentrations of HRP

4 and various concentrations of H₂O₂ ranging from 1 mM to 1 µM to find a limit of detection of the

5 silk fibroin mats with quantification of the change of the color intensity done by ImageJ software.

6 A) Control and Amplex infused silk fibroin mats in the presence of a fixed HRP concentration of

7 25 µg/mL and various H₂O₂ concentrations at 30-minute, 24-hour, and 48-hour time point. B)

8 Control and Amplex infused silk mats in the presence of a fixed HRP concentration of 0.25 µg/mL

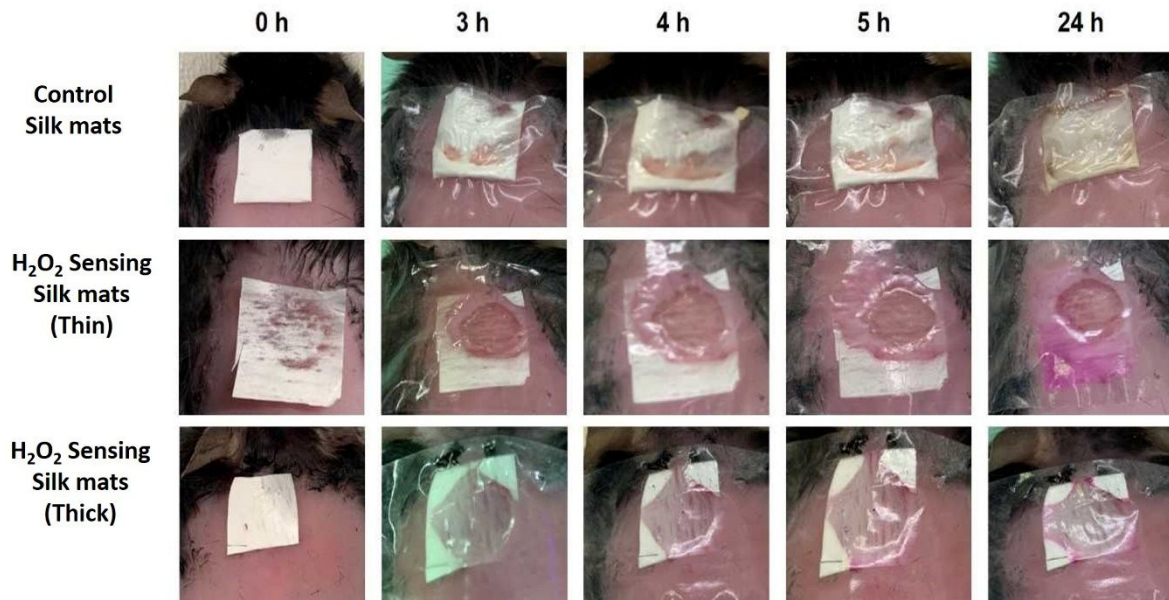
9 and various H₂O₂ concentrations at 30-minute, 24-hour, and 48-hour time points. C) Quantification

1 of color intensity for the mats treated with 0.25 $\mu\text{g}/\text{mL}$ HRP at the 24-hour time point. D)
2 Quantification of color intensity for the mats treated with 0.25 $\mu\text{g}/\text{mL}$ HRP at the 48-hour time
3 point.

4 **3.3 *In-vivo* cutaneous wounds testing for visible sensing of oxidative stress.** Visible color
5 development in the amplex infused nanofibrous silk fibroin mats were observed, verifying
6 the proof of concept developed for color sensing mats for reactive oxygen species.
7 Further, in order to evaluate the change in color of these sensing mats in the wound
8 directly, we applied the amplex infused nanofibrous silk fibroin mats, both thin and thick,
9 on diabetic mouse wounds. In terms of thickness, the silk fibroin nanofibrous thin mats
10 were 0.001 mm thick, while the silk fibroin nanofibrous thick mats were 0.0043 mm thick,
11 indicating a 4-fold difference in terms of thickness among both mats. These silk fibroin
12 mats including control mats were placed onto the wounds and observed for 24 hours a
13 for visible ROS sensing and color change. The amplex infused silk fibroin mats were
14 found to be absorbing the wound exudates and developed the visible pink color due to
15 ROS sensing over a period of 24 hours, indicating its effectivity and sensitivity as

1 compared to control mats which remained colorless. The thin mats were more
2 pronounced in color development (**Figure 7**). This might be due to the fact that these thin
3 mats are almost 4-fold less dense than thick mats and have gotten saturated with the
4 wound exudates containing peroxidase and H_2O_2 , leading to the faster oxidation of
5 amplex red into resorufin and yielding purple color.

6



1

2 **Figure 7:** H₂O₂ color sensing with amplex infused silk fibroin mats were performed using a diabetic

3 (Db/Db) mouse model of wound healing. In these in vivo study, control silk fibroin mats, H₂O₂

4 color sensing silk fibroin mats (Thin ~0.001mm thickness) and H₂O₂ color sensing silk fibroin

5 mats (Thick ~ 0.0043 mm thickness) i.e amplex Infused silk fibroin mats were used. 8 mm dermal

6 wounds were created onto the skin of diabetic mice these mats were applied respectably. Upon

7 observation it was noted that, within 24 hrs of time period the H₂O₂ color sensing silk fibroin mats

8 white color changed to pink color due to the encountering of H₂O₂ oxidative molecules and

9 peroxidase exuding from the wound site, indicating the high concentration over 24 hrs time

10 period.

1 The wound release exudates which include a variety of enzymes like peroxidases and
2 biochemicals including oxidative stress-inducing factors like H_2O_2 , OH, and others. This
3 is where the amplex incorporated into the silk fibroin mat would get oxidized into visible
4 resorufin and can be visibly observed. Overall, the level of visible detection of amplex
5 infused silk fibroin mats were accurate even at low concentration. However, this is
6 indicated for the current 1 mL of 5 mg/mL of amplex infused into the nanofibrous silk
7 fibroin mats. Future studies will be carried out to determine the amplex loading capacities
8 onto these nanofibrous silk fibroin mats and identify its sensitivity in H_2O_2 detection.

9 4. CONCLUSION

10 In conclusion, we were able to electrospin nanofibrous silk fibroin mats through the
11 processing of silk fibroin solution directly from the raw silk cocoons. These nanofibrous
12 silk fibroin mats were infused with amplex red dye for a real-time sensing of the oxidative
13 stress in the wounds through the oxidation of amplex into resorufin by H_2O_2 moiety. FTIR
14 analysis confirmed the amplex red infusion into these fine nanofibers and the chemical
15 integrity into the mats post electrospinning. *In vitro* color sensing experiments indicated

1 that concentrations of H₂O₂ as low as 25 μm with 0.25 μg/mL of HRP can easily produce
2 a visible color change. *In vitro* cellular biocompatibility was also observed for the mats
3 and further *in vivo* experiments were performed using the diabetic wounds, which
4 indicated the visible color sensing mats after a 24 hour incubation time period, indicative
5 of sensing oxidative stress in these wounds. These H₂O₂ sensing mats would be ideal to
6 monitor the changes in oxidative stress and ROS levels directly in the wounds and may
7 help allow the adaptation and personalization of treatment based on the levels of oxidative
8 stress of each wound.

9

10 **AUTHORS CONTRIBUTION**

11 S.S, G.C performed the materials synthesis and *in vitro* experiments. U.K, and T.S.S
12 performed the materials characterization. S.M.N., A.E.L., M.A.B., and C.Z performed the
13 *in vivo* experiments. S.S analyzed the data and wrote the manuscript. K.W.L, and S.S
14 conceived the idea. All authors reviewed and commented on the manuscript.

15 **CONFLICTS OF INTERESTS**

1 The authors declare that there is no conflict of interest regarding the publication of this article.

2

3 ACKNOWLEDGMENT

4 The authors gratefully acknowledge the support of Material Characterization Facility (MCF)
5 provided by the Advanced Materials Processing and Analysis Center and Material Science and
6 Engineering Department for the characterization of different material employed in this manuscript.

7 The authors also acknowledge the funding from NSF MRI XPS: ECCS#1726636 for XPS
8 measurement, NSF REU: EEC#1560007, & UCF Trustee chair award.

9

10 REFERENCE

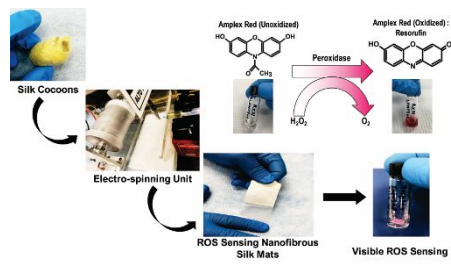
- 11 1. G. Han and R. Ceilley, *Advances in Therapy*, 2017, **34**, 599-610.
- 12 2. G. Sener, S. A. Hilton, M. J. Osmond, C. Zgheib, J. P. Newsom, L. Dewberry, S.
13 Singh, T. S. Sakthivel, S. Seal, K. W. Liechty and M. D. Krebs, *Acta*
14 *Biomaterialia*, 2020, **101**, 262-272.
- 15 3. M. B. Dreifke, A. A. Jayasuriya and A. C. Jayasuriya, *Materials Science and*
16 *Engineering: C*, 2015, **48**, 651-662.
- 17 4. H. Wu, F. Li, S. Wang, J. Lu, J. Li, Y. Du, X. Sun, X. Chen, J. Gao and D. Ling,
18 *Biomaterials*, 2018, **151**, 66-77.
- 19 5. H. Steiling, B. Munz, S. Werner and M. Brauchle, *Experimental cell research*,
20 1999, **247**, 484-494.
- 21 6. T. A. Wilgus, S. Roy and J. C. McDaniel, *Advances in wound care*, 2013, **2**, 379-
22 388.

- 1 7. T. Pirmohamed, J. M. Dowding, S. Singh, B. Wasserman, E. Heckert, A. S.
2 Karakoti, J. E. King, S. Seal and W. T. Self, *Chemical communications*, 2010, **46**,
3 2736-2738.
- 4 8. H. M. Kimmel, A. Grant and J. Ditata, *Wounds: A compendium of clinical*
5 *research and practice*, 2016, **28**, 264-270.
- 6 9. M. Mittal, M. R. Siddiqui, K. Tran, S. P. Reddy and A. B. Malik, *Antioxidants &*
7 *redox signaling*, 2014, **20**, 1126-1167.
- 8 10. P. D. Ray, B.-W. Huang and Y. Tsuji, *Cellular signalling*, 2012, **24**, 981-990.
- 9 11. D. J. Betteridge, *Metabolism*, 2000, **49**, 3-8.
- 10 12. C. K. Sen and S. Roy, *Biochimica et Biophysica Acta (BBA)-General Subjects*,
11 2008, **1780**, 1348-1361.
- 12 13. X. Wang, M. K. Sng, S. Foo, H. C. Chong, W. L. Lee, M. B. Y. Tang, K. W. Ng, B.
13 Luo, C. Choong and M. T. C. Wong, *Journal of controlled release*, 2015, **197**,
14 138-147.
- 15 14. J.-I. Jun and L. F. Lau, *Nature cell biology*, 2010, **12**, 676.
- 16 15. E. Aliyev, U. Sakallıoğlu, Z. Eren and G. Açıkgöz, *Biomaterials*, 2004, **25**, 4633-
17 4637.
- 18 16. Y.-H. Lee, J.-J. Chang, C.-T. Chien, M.-C. Yang and H.-F. Chien, *Experimental*
19 *diabetes research*, 2012, **2012**.
- 20 17. K. K. Griendling, R. M. Touyz, J. L. Zweier, S. Dikalov, W. Chilian, Y.-R. Chen, D.
21 G. Harrison and A. Bhatnagar, *Circulation research*, 2016, **119**, e39-e75.
- 22 18. S. Dikalov, K. K. Griendling and D. G. Harrison, *Hypertension*, 2007, **49**, 717-
23 727.
- 24 19. D. Dębski, R. Smulik, J. Zielonka, B. Michałowski, M. Jakubowska, K. Dębowska,
25 J. Adamus, A. Marcinek, B. Kalyanaraman and A. Sikora, *Free Radical Biology*
26 *and Medicine*, 2016, **95**, 323-332.
- 27 20. W. M. Aumiller Jr, B. W. Davis, N. Hashemian, C. Maranas, A. Armaou and C. D.
28 Keating, *The Journal of Physical Chemistry B*, 2014, **118**, 2506-2517.
- 29 21. B. Zhao, F. A. Summers and R. P. Mason, *Free radical biology and medicine*,
30 2012, **53**, 1080-1087.

- 1 22. C. Holland, K. Numata, J. Rnjak-Kovacina and F. P. Seib, *Advanced healthcare*
2 *materials*, 2019, **8**.
- 3 23. D. N. Rockwood, R. C. Preda, T. Yücel, X. Wang, M. L. Lovett and D. L. Kaplan,
4 *Nature protocols*, 2011, **6**, 1612.
- 5 24. S. Aziz, M. Sabzi, A. Fattahi and E. Arkan, *Journal of Polymer Research*, 2017,
6 **24**, 140.
- 7 25. S. Singh, A. Ly, S. Das, T. S. Sakthivel, S. Barkam and S. Seal, *Artificial cells,*
8 *nanomedicine, and biotechnology*, 2018, 1-8.
- 9 26. N. Saraf, S. Barkam, M. Pepler, A. Metke, A. Vázquez-Guardado, S. Singh, C.
10 Emile, A. Bico, C. Rodas and S. Seal, *Sensors and Actuators B: Chemical*, 2019,
11 **283**, 724-730.
- 12 27. A. J. Meinel, K. E. Kubow, E. Klotzsch, M. Garcia-Fuentes, M. L. Smith, V. Vogel,
13 H. P. Merkle and L. Meinel, *Biomaterials*, 2009, **30**, 3058-3067.
- 14 28. C. Li, C. Vepari, H.-J. Jin, H. J. Kim and D. L. Kaplan, *Biomaterials*, 2006, **27**,
15 3115-3124.
- 16 29. H.-J. Jin, S. V. Fridrikh, G. C. Rutledge and D. L. Kaplan, *Biomacromolecules*,
17 2002, **3**, 1233-1239.
- 18 30. L. Huang, K. Nagapudi, R. P. Apkarian and E. L. Chaikof, *Journal of Biomaterials*
19 *Science, Polymer Edition*, 2001, **12**, 979-993.
- 20 31. L. G. Griffith, *Acta Materialia*, 2000, **48**, 263-277.
- 21 32. V. Mishin, J. P. Gray, D. E. Heck, D. L. Laskin and J. D. Laskin, *Free Radical*
22 *Biology and Medicine*, 2010, **48**, 1485-1491.
- 23 33. S.-H. Kim, B. Kim, V. K. Yadavalli and M. V. Pishko, *Analytical Chemistry*, 2005,
24 **77**, 6828-6833.
- 25 34. V. W. Wong, K. C. Rustad, J. P. Glotzbach, M. Sorkin, M. Inayathullah, M. R.
26 Major, M. T. Longaker, J. Rajadas and G. C. Gurtner, *Macromolecular*
27 *Bioscience*, 2011, **11**, 1458-1466.
- 28 35. L. S. Gloyne, G. D. Grant, A. V. Perkins, K. L. Powell, C. M. McDermott, P. V.
29 Johnson, G. J. Anderson, M. Kiefel and S. Anoopkumar-Dukie, *Toxicology in*
30 *Vitro*, 2011, **25**, 1353-1358.

- 1 36. Y. D. Shanskii, N. Sergeeva, I. Sviridova, M. Kirakozov, V. Kirsanova, S.
2 Akhmedova, A. Antokhin and V. Chissov, *Bulletin of experimental biology and*
3 *medicine*, 2013, **156**, 146-151.
- 4 37. K. Min, S. Kim, C. G. Kim and S. Kim, *Scientific reports*, 2017, **7**, 5448.
- 5 38. J. Doshi and D. H. Reneker, *Journal of electrostatics*, 1995, **35**, 151-160.
- 6 39. S. V. Fridrikh, H. Y. Jian, M. P. Brenner and G. C. Rutledge, *Physical review*
7 *letters*, 2003, **90**, 144502.
- 8 40. X. Zhang, M. R. Reagan and D. L. Kaplan, *Advanced drug delivery reviews*,
9 2009, **61**, 988-1006.
- 10 41. H. Wang, H. Shao and X. Hu, *Journal of Applied Polymer Science*, 2006, **101**,
11 961-968.
- 12 42. M. Boulet-Audet, F. Vollrath and C. Holland, *Journal of Experimental Biology*,
13 2015, **218**, 3138-3149.
- 14 43. D. J. Belton, R. Plowright, D. L. Kaplan and C. C. Perry, *Acta biomaterialia*, 2018,
15 **73**, 355-364.
- 16 44. X. Hu, D. Kaplan and P. Cebe, *Macromolecules*, 2006, **39**, 6161-6170.
- 17 45. T. C. D. Fernandes, H. M. R. Rodrigues, F. A. A. Paz, J. F. M. Sousa, A. J. M.
18 Valente, M. M. Silva, V. de Zea Bermudez and R. F. P. Pereira, *Journal of The*
19 *Electrochemical Society*, 2020, **167**, 070551.
- 20 46. J. Shao, J. Liu, J. Zheng and C. M. Carr, *Polymer international*, 2002, **51**, 1479-
21 1483.
- 22 47. Q. Wang, R. Yanzhang, Y. Wu, H. Zhu, J. Zhang, M. Du, M. Zhang, L. Wang, X.
23 Zhang and X. Liang, *RSC advances*, 2016, **6**, 34219-34224.
- 24 48. I. Dal Pra, A. Chiarini, A. Boschi, G. Freddi and U. Armato, *International journal*
25 *of molecular medicine*, 2006, **18**, 241-247.
- 26 49. K.-H. Kim, L. Jeong, H.-N. Park, S.-Y. Shin, W.-H. Park, S.-C. Lee, T.-I. Kim, Y.-
27 J. Park, Y.-J. Seol and Y.-M. Lee, *Journal of biotechnology*, 2005, **120**, 327-339.

Table of content



Amplex red infused silk mats in visible detection of oxidative stress in the cutaneous wound over time